Defect growth in multilayer chromium nitride/niobium nitride coatings produced by combined high power impulse magnetron sputtering and unbalance magnetron sputtering technique

BISWAS, Barnali, PURANDARE, Yashodhan <http://orcid.org/0000-0002-7544-9027>, ARUNACHALAMSUGUMARAN, Arunprabhu <http://orcid.org/0000-0002-5087-4297>, LOCH, Daniel <http://orcid.org/0000-0003-3252-0142>, CREASY, Stuart, KHAN, Imran, EHIASARIAN, Arutiun <http://orcid.org/0000-0001-6080-3946> and HOVSEPIAN, Papken <http://orcid.org/0000-0002-1047-0407>

Defect growth in multilayer Chromium Nitride/Niobium Nitride coatings produced by combined High Power Impulse Magnetron Sputtering and Unbalance Magnetron Sputtering technique

Running title: Growth defects in HIPIMS/UBM CrN/NbN multilayer coatings

Running Authors: Biswas et al.

Barnali Biswas [a)], Yashodhan Purandare, Arunprabhu A. Sugumaran, Daniel A.L. Loch, Stuart Creasey, Arutiun P. Ehiasarian, Papken Eh. Hovsepian

National HIPIMS Technology Centre, Materials and Engineering Research Institute, Sheffield Hallam University, City Campus, Howard Street, Sheffield S1 1WB, United Kingdom

Imran Khan

Zimmer-Biomet UK Limited, Dorcan Industrial Estate, Murdoch Road, Swindon - SN3 5HY, United Kingdom

[a)] Corresponding author: Barnali.Biswas@student.shu.ac.uk

In recent years, high power impulse magnetron sputtering (HIPIMS) has caught the attention of users due to its ability to produce dense coatings. However, microscopic studies have shown that HIPIMS deposited coatings can suffer from some surface imperfections even though the overall number of defects can be significantly lower compared to, for example, arc deposited coatings of similar thicknesses. Defects can degrade the coating performance thus any kind of defect is undesirable. To better understand the nature of these imperfections and the science of their formation, a series of Chromium Nitride/Niobium Nitride (CrN/NbN) coatings were deposited using HIPIMS technique combined with unbalanced magnetron sputtering (UBM) by varying deposition times (t = 15 to 120

minutes). All other deposition parameters were kept constant in order to deposit these coatings with a consistent deposition rate and stoichiometry.

In addition, coatings were deposited using pure UBM technique to compare the defects generated by these two different physical vapour deposition approaches. High-resolution scanning electron microscopy images revealed that HIPIMS/UBM and pure UBM CrN/NbN coatings have similar types of defects which could be categorised as: nodular, open void, cone-like and pinhole. Interestingly, there was no evidence of droplet formation in HIPIMS/UBM deposited coatings.

The defect density calculation indicated that the defect density of HIPIMS/UBM coatings increased (from 0.48 to 3.18%) with the coating thickness. A coating produced in a relatively clean chamber had a lower defect density. Potentiodynamic polarisation experiments showed that the fluctuation in corrosion currents in HIPIMS/UBM coatings reduced with the coating thickness. This indicated that though visible on the surface, most of these defects did not penetrate thorough the whole thickness of the coating.

Keywords: HIPIMS, CrN/NbN, Microstructure, Growth defects, Defect density, Corrosion.

1. Introduction

The attention towards the physical vapour deposition (PVD) techniques is increasing as this technique is more environment-friendly when compared to electroplating deposition and it can produce sustainable coatings for various applications [1]. However, PVD coatings are not free from growth defects or imperfections and these growth defects can degrade the coating performance [2–10]. The most commonly and industrially used PVD technique, arc-PVD, itself creates droplets which initiate the defects generation in the coatings [5–7,11–13].

The high power impulse magnetron sputtering (HIPIMS) technique has been proven useful in depositing coatings as dense as arc-PVD [14]. This novel technique boosts the generation of metal ions and ions of reactive gases in the plasma which is free from droplet phase when operated under carefully selected parameters, such as the right frequency, pulse width and arc suppression settings [15]. It has been widely published that the HIPIMS technique is an excellent tool for the deposition of coatings with very dense structure without inter-columnar voids but shows a relatively lower deposition rate, whereas the unbalanced magnetron sputtering (UBM) technique has a high deposition rate but can produce porous coatings [15–19]. A combination of both techniques, however can eradicate these problems and produce coatings with a high deposition rate and very dense structure [16,20].

Previous studies have shown that defects in PVD coatings can be generated due to external factors. For example, contamination of the depositing surface with dust (loose particles of metal/metal-compounds) often generated due to the thermal expansion of chamber components (common for any coating technique associated with vacuum chambers) and

substrate irregularities like pits can initiate defect formation [2,3,9,10]. Defects generated during coating growth using HIPIMS have not been discussed in detail. However, this is of particular interest for HIPIMS, as high power densities are used for etching, and deposition is carried out in highly reactive plasma with very dynamic target poisoning conditions. This study investigates the defect formation at different steps during Chromium Nitride/Niobium Nitride (CrN/NbN) coating deposition by HIPIMS/UBM technique carried out in optimised conditions and attempts to identify the source of those defects and to understand their formation.

For this study the CrN/NbN coating was considered because of its wide industrial applications in recent years as a protective material due to the high hardness, good wear resistance and anticorrosive properties [1,21,22]. The excellent performance of nanoscale CrN/NbN coatings in various applications such as pump impellers, hydraulic valves, nozzles, pistons and sharp edges (cutting blades) has been previously demonstrated [22–24]. Surface imperfections have not proved to be detrimental in any of the above mentioned applications; however advanced coating applications (biomedical and industrial) demands thorough investigation of the growth defects to aid better understanding of their influence on the overall coating performance. Literature available on the defects associated with HIPIMS coatings is very rare, and is the motivation behind this work.

2. Experimental details

2.1 Coating deposition

2.1.1 HIPIMS/UBM Coating:

CrN/NbN nano-structured multilayer coatings were deposited in an industrial sized machine (Hauzer 1000 four target PVD system) using the combined HIPIMS/UBM technique. The machine has a chamber size of 1 m^3 with four rectangular planar targets (sized 600 x 200 mm). In this study the machine was equipped with two HIPIMS power supplies (Hüttinger Elektronik Sp. z o.o., Warsaw, Poland) and a dedicated bias power supply which had active arc suppression units on cathode and substrate bias supplies. The deposition system has four cathodes furnished with two Chromium (Cr) and two Niobium (Nb) targets. Prior to the deposition, the substrate surfaces were pre-treated with a HIPIMS plasma discharge enriched with Cr ions to improve the adhesion of the coating with the substrate [14,19,25]. Finally a CrN/NbN superlattice nano-scale multilayer coating was deposited at a bias voltage of U_B= - 65 V in a combined Ar and N_2 (1:1) atmosphere. During this nanoscale multilayer coating deposition step, one Cr and one Nb target were operated in HIPIMS mode, while the other two targets (1 Cr and 1 Nb) were operated in UBM mode. The machine was operated in the constant power mode where the average power on the target(s) was always maintained at 8 kW irrespective of the technology (UBM or HIPIMS). Rectangular pulses of 200 µs at a frequency of 100 Hz, with a peak current of 400 A and duty cycle of 1% were employed to generate the HIPIMS plasma for coating deposition. The distance between targets and substrate holder was 155 mm. During all deposition processes, the deposition temperature and chamber pressure were maintained at 200 $^{\circ}$C and at 35 Pa respectively. In this study the deposition time was varied and ranged from 15 to 120 minutes. To produce homogeneous coatings, samples were mounted onto a three-fold rotational substrate holder.

2.1.2 UBM Coating:

During pure UBM coating deposition, all four targets were operated in UBM mode. The maximum deposition time for the coating was 100 min. The chamber pressure and temperature were maintained as stated above. Coupons of 304 stainless steel and (100) Silicon wafers were used as substrates. The 304 stainless steel substrates were polished to a mirror finish (R_a= 0.01 µm). The polished samples and the Silicon wafers were cleaned in an automated ultrasonic cleaning line with industrial detergents (alkaline cleaning agents from borer chemicals) to remove surface contaminants.

2.2 Microstructural Investigation

2.2.1. Atomic Force Microscopy

Anton Paar- CSM atomic force microscope (AFM) was used to examine the surface morphology. The AFM produced topographical images by scanning over the sample surface using a silicon nitride stylus with a probe tip (operated by CSM software).

2.2.2. Scanning electron microscopy

Scanning electron microscopy (FEI-Nova NanoSEM 200) was used to capture the secondary electron (SE) images of planar and fractural cross sectional view of the coatings. The working distance was in the range of 4 to 5 mm and the beam voltage was in the range of 5 to 20 kV in the process to capture clear images. At lower magnification ETD (Everhart-Thornley detector) was used whereas TLD (Through the Lens Detector) was used to capture images at high magnification.

FEI Quanta 650 3D DualBeam FIB FEG-SEM was used to produce cross sections of specific growth defects on the surface and obtain high-quality images. The Quanta 3D used for this study is a combination of two systems: a focused ion beam (FIB) comprising of Gallium (Ga) ion gun system and a field emission gun (FEG). During milling 30 kV voltage was applied. After milling, ETD was used to capture the cross sectional SEM images of the defects. The working distance was fixed at 10 mm and the applied voltage was 10 kV.

2.2.3. Optical Microscopy

Huvitz 3D optical microscope and ImageJ software were used to analyse the percentage of surface area of the sample covered with imperfections (i.e. the defect density in the coating). The optical microscope (OM) used to examine the surface of the coating was equipped with a Plan Fluor semi Apochromat optical lens with a magnification of 100×. Then the images of the coating surfaces (130 µm × 90 µm) were captured using a digital camera at a magnification of 1000 times. For each coating, ten images were captured. ImageJ software was used to convert those optical microscopic images into black and white binary images. As a result, the pronounced surface imperfections (growth defects, droplets) appeared as prominent black features with respect to the now white background. Using the software, the number of droplets and the percentage of the sample area covered by these surface imperfections, were determined to calculate the average value of the defect density for each coating.

2.3 Topographical studies

A stylus profilometer (DEKTAK 150) was used to measure the surface roughness of polished substrates as well as deposited coatings by scanning a diamond stylus over the surface. The radius of the stylus was 12.5 µm and 4 mg load was applied on it during all scans. For each sample five scans was recorded. During these scans the probe travelled a length of 1000 µm of the surface profile with a spatial resolution of 0.033 µm and the surface roughness of the scanned profile was calculated by the associated software. Roughness values were calculated by averaging all five scans.

2.4 Corrosion studies

In order to examine the Corrosion behaviour of the coatings, potentiodynamic polarisation studies were carried out using Gill AC Potentiostat. All electrochemical experiments were performed in a 3.5% NaCl solution at room temperature in order to examine the pitting behaviour. The exposed surface area of the coated CrN/NbN 304 stainless steels was 1 cm^2. The corrosion tests were conducted by polarising the sample from -1000 mV to +1000 mV at a scan rate of 0.5 $mVsec^{-1}$. After corrosion tests, optical microscopic images were captured to examine any changes in the condition of the surfaces.

3. Results and discussion

3.1 Topographical and microstructural results of coating surfaces

Topography and microstructure of the etched substrate and the coating surface were studied using AFM and SEM techniques. Fig. 1a shows a 2D AFM image of the Cr ion etched

substrate surfaces over an area of 20×20 μm^2. The colour intensity shows the surface profile of the coatings with the lighter shaded regions being the highest points and the darker shaded regions being associated with pores and cavities. The image shows cavities and scratches produced during the mechanical polishing step of the samples. Although during the HIPIMS etching step, when a thin surface layer (a few nm) is removed by sputtering from the bombardment of accelerated Cr ions, a complete removal of all surface imperfections is not achieved as the etching process itself is not meant to be very aggressive. Therefore, surface defects such as pinholes and scratches inherited from the substrate were apparently visible (Fig. 1a) even after the etching step. These defects are regarded as one of the main sources /sites for generation of [2,3].

Low magnification SEM image of the same ion etched substrate but different area (Fig. 1b) shows no evidence of droplet formation when HIPIMS was used for etching. This is in stark contrast to an cathodic arc etched surface where, at the end of the etching step the surface is covered with droplets [5–7]. This superior surface finish after HIPIMS etching was a result of careful parameter selection and effective use of arc suppression units on cathodes and bias power supplies [15,16,19]. However, the surface roughness associated with the preferential etching of the grain boundaries and protruding grains was clearly visible in the high magnification SEM image (Fig. 1c).

Fig. 2a-h show the AFM and SEM images of the coated surface deposited by HIPIMS/UBM with varying deposition time. For the 15 minutes deposited coating (Fig. 2a,b), it was evident that the coating deposition had started and covered the surface extensively. However, the imprints of preferential etching of the substrate can still be

observed even after a coating thickness of 0.28 µm. Coating morphology, which was dependent on both the grain orientation and grain size of the substrate, suggested a high epitaxy in coating growth, which is a finger print of HIPIMS [15,16,19,26].

For 30 minutes deposition time, (Fig. 2c), most of the surface was covered with coating flux engulfing most of the smaller substrate imperfections, however imprints of some of the deep scratches and pits were still visible as the coating simply follows the topography. With an increase in the deposition time and thereby of coating flux, for e.g. 60 minutes of deposition (Fig. 2e-f), the majority of the surface imperfections were found to be covered and infused within the coating [2,3] and the morphology appeared more homogeneous. Growth of a columnar structure with rounded column tops (typical for sputter coatings) could be observed (plan view of the coating surface in Fig. 2f) with a difference that the coating structure was found to be homogeneous, densely packed and fine grained in the cross-sectional microscopic studies conducted (Fig. 5a) and can be attributed to the high energy ion bombardment from the HIPIMS plasma. This is significant since low substrate bias voltages and low deposition temperature (200 °C) were used. Some evidence of contamination defects (explained in the following sections) was also evident.

For 120 minutes deposition time, (Fig. 2g,h), the basic columnar morphology remained unchanged, however the grain size increased noticeably; more peculiar dome shaped column tops were visible. In this study, two targets were running in HIPIMS mode and two other targets were operated in UBM mode. The benefit of using HIPIMS was clearly visible as the columns were found to be very densely packed (Fig. 5a) than would be for pure UBM deposited coating deposited in similar conditions [27].

Although the coating morphology becomes homogeneous with the increase of deposition time, the larger cavities on the substrate surface may never get covered with the coating materials if the coating is thin especially when conditions such as atomic shadowing dominate. These cavities can be apparent on the surface of the fully grown coating, as was visible in the case of 120 minutes deposited coating (Fig. 2g).

3.2 Growth Defects

Defect formation in PVD coatings is well known and has been described before by various authors [2–10].They have systematically defined the defects according to their size and shape. In this research extensive SEM studies were conducted to investigate the defects in HIPIMS/UBM deposited CrN/NbN coatings. The types of defects identified were very similar in nature to those reported earlier for a conventional magnetron sputtering process [2,3,9,10]. For clarity, a short description of each defect type, the mechanism of their formation and corresponding SEM images (Fig. 3a-f) of the defects observed in this study of HIPIMS/UBM deposited and UBM deposited CrN/NbN coatings is briefly given below:

Nodular defects: A magnified image of a nodular defect is shown in Fig. 3a. These defects are associated with foreign particles (flakes) which arise from the inner surfaces of the vacuum chamber (shields, heaters and other components). They are attached but not strongly bonded to the substrate surface. Subsequent coating deposition on these particles produces nodular defects [2,3,7,8,26]. A significant difference between arc droplet and a nodular defect is that the coating growth over time (in the form of columnar grains) within the defect can be clearly seen for nodular defects whereas arc droplets either solidify outside the coating or on the surface instantaneously.

Open void defects: Fig. 3b shows the image of an open void defect with a flake residue and a subsequent crater formed. These types of defects form by a spontaneous 'flaking off' of lightly attached nodular defects and this 'flaking off' can occur during both coating growth and the cooling process [2].

Pinhole defects: Fig. 3c shows the magnified image of the cavity (dark contrast area) with a lack of coating material and can be classified as a pinhole defect. These kinds of defects extend through the whole coating from substrate to the top surface of the coating.

Cone-like defects: Fig. 3d shows a cross sectional view of a cone-like defect. Like a nodular defect, the origin of these defects is also foreign particles. However, in this case those particles get attached to the substrate at a very initial stage of coating deposition and produce cone-like structure within the coating. Same kind of defects can be formed on small protrusions on the substrate surface which exist on most of the engineering surfaces inherited from their manufacturing technique [2]. A detailed description of these defects can be found in another article [26].

In this study, it was found that the defects observed in HIPIMS/UBM deposited coatings were similar to those observed for pure UBM deposition i.e. defects which were common to any sputtering process and related to contamination arising from the surrounding chamber walls and fixtures. Thus it is appropriate to conclude that the use of the HIPIMS technique did not lead to the generation of a new type of defect. Extensive SEM studies, like represented in Fig. 1b-c, Fig. 2b,d,f,h and Fig. 3f clearly showed that, neither in the etching stage nor in the deposition stage, any droplet defects were formed on the surface. This is significant for a sputtering technique since low deposition temperatures and high power

densities were used for coating deposition and also due to the fact that HIPIMS plasma is highly reactive and ionised which makes target poisoning phenomena extremely complex [16,20,28].

For comparison, plan views of a HIPIMS/UBM CrN/NbN coating and an arc-PVD CrN/NbN coating of similar thicknesses have been shown in Fig. 3f and Fig. 3g respectively. It is clearly visible that arc-PVD coatings (Fig. 3g) have a higher number of defects compared to HIPIMS/UBM coatings (Fig. 3f). Also the defects on arc-PVD coating are larger in size. The more detailed observation of the SEM images of a nodular defect of HIPIMS/UBM coating (Fig. 3a) and the droplet defect of an arc-PVD coating (Fig. 3h) demonstrates the structural difference of both kinds of defects. The nodular defect is believed to be formed due to the deposition of coating materials on the top of foreign particles attached to the substrate whereas the cluster of materials ejected from the target leads to droplet formation in arc-PVD.

Thus we can conclude that careful selection of deposition parameters such as pulse frequency and duration along with the effective use of arc suppression units on HIPIMS power supplies as well as bias power supplies prevent the formation of arc droplet defects [19]. Furthermore the highly ionised HIPIMS plasma helped to produce very dense coatings thus eliminating any intercolumnar voids or generation of under dense structures or large pinholes as observed for pure UBM coating in this study (Fig. 3e).

To investigate the core structure of defects, cross-sectional FIB-SEM images of the above mentioned growth defects were studied. Fig. 4a shows a planar view of a nodular defect, whilst Fig. 4b shows the cross sectional view of the defects after ion beam milling which

indicates that the defect started to grow after a certain deposition time. A thin layer of deposited coating was visible between the defect and the substrate. The void between the defect and the rest of the coating thickness was clearly visible in the detail SEM view (Fig. 4c) of the same defect. Due to the loose bonding of the nodular defects with respect to the rest of the coating, these defects can be easily detached during post deposition applications due to stresses (thermal or mechanical). Removal of such defects creates pits on the coating surface and reduces the effective thickness of the coating. The lower thickness can make coating less protective and the pits may act as a pathway for corrosive media to reach the substrate. Hence, these growth defects are more likely to lead to severe degradation of the coating under load and corrosion attack.

3.3 Effect of coating thickness on the defect formation and defect density

The cross-sectional SEM images of the nodular defects suggested that most of the defects were generated around the intermediate stages of coating growth. Results presented in Fig. 2a-h suggests that the critical time required for contamination related defects (foreign particles such as flake and chamber dust) to appear was between 30 and 60 minutes of deposition. As stated earlier, this study also investigated the effect of deposition time on the defect density. The coating thickness was measured on fractured Silicon wafer cross-sections using SEM. For each coating five images were captured and the average value of thickness was calculated. The thickness values were found to be 0.28 µm (15 minutes deposition), 0.56 µm (30 minutes deposition), 1.26 µm (60 minutes deposition) and 2.15 µm (120 minutes deposition). Fig. 5a shows the coating thickness as a function of the deposition time. Relevant cross section SEM images are included in insets to support the

thickness data. As expected, the coating thickness increased with the deposition time exhibiting a linear relationship. This indicates constant coating deposition conditions and deposition rate, which was calculated to be 0.018 µm per minute. Thickness for UBM coating was 2.1 µm (100 minutes deposition) (Fig. 5b).

Images captured by the Huvitz microscope and the Image J software were used to study the relationship between deposition time and defect density visible on the surface. The defect density (A_d) was calculated as a percentage of the surface area covered by imperfections of a coated sample. Fig. 6 shows the relationship between the defect densities to the coating thickness. It can be clearly observed that there was a direct proportionality between these two factors; as the coating thickness increased the area percentage of growth defects also increased. The increase in growth defect density with time was assumed to be due to the increase of the number of small flakes (seed) in the chamber during the deposition process. Some of the seed particles generate from the chamber components of the coating system due to the thermal and structural stresses or the ion-bombardment on them. Further sources for small seed particles and wear debris are the sputter flux bombardment on chamber and the rotation of the substrates holders. The Combination of all these mechanisms, increase the amount of flakes in the chamber with time. When flakes of significant size fall on the substrate, they may effectively alter the coating growth direction as compared to that of the rest of the coated surface, thus forming nodular defects [2,3]. During or after the deposition, some nodular defects can be expelled due to high compressive stresses present in them thus creating a different type of defect such as cavities. For comparison, a 3 µm thick arc deposited CrN/NbN coating (commercially available) was also investigated. Results

exhibited that the arc-PVD CrN/NbN coating had the highest defect density (10.85%) which can be mainly attributed to the droplet defects.

As the flakes from chamber components are believed to be the reason for the most of defects generated in the case of HIPIMS/UBM coatings, additional studies were conducted to see the effect of clean environment on the defect density. Hence, coatings were deposited using HIPIMS/UBM and pure UBM techniques after the chamber parts were cleaned. As anticipated, the defect density of the coating produced by HIPIMS/UBM technique in a clean chamber reduced (1.37% as compared to 3.18% before cleaning) even though it was thicker (2.36 µm). The UBM coating (thickness = 2.10 µm) also had lower defect density (0.21% as compared to 0.87% before cleaning) on its surface. The reason behind the lower defect density in UBM coating can be attributed to the low energetic particles in the plasma during UBM deposition which results in fewer seed particles generated by the bombardment of the chamber walls.

Table 1 presents the results from surface roughness (R_a, µm) measurements of the polished substrate and deposited coating surfaces. As expected the R_a value of the polished substrate was measured to be the lowest (0.012 µm). The surface roughness R_a increased rapidly by a factor of two (R_a = 0.023 µm) when the samples were subjected to the etching process. This can be explained by the substrate material removal by the sputtering caused by the bombardment with the high energy ions generated in the HIPIMS discharge. This sputtering can be aggressive in some places, e.g. - grain boundaries or specific microstructural phases as compared to other which give rises to an uneven surface on a nanometer scale.

During the analysis of the 15 minutes deposited coating, it was observed that the roughness value initially decreased slightly (0.021 μm) due to the covering of the uneven surface by the depositing material. However, further increase of the deposition time led to increase of the surface roughness. For the maximum deposition time of 120 minutes, the roughness value, R_a was observed to be the highest (0.039 μm). This behaviour was attributed to the natural increase in column diameter and their dome shaped tops with the increase of the coating thickness which is typical for a competitive coating growth mechanism [29].

The reproduced HIPIMS/UBM coating (deposition time 120 minutes) deposited in a cleaner chamber, had lower roughness value, 0.031 μm. The difference in roughness values of HIPIMS/UBM coatings (with the same deposition time) and that of pure UBM coating indicates the dependency of surface roughness on growth defects as well as on the microstructure of the coating.

3.4 Potentiodynamic polarisation results

It has been suggested that, the corrosion performance of CrN/NbN superlatices is a function of their chemical composition, residual stress levels and growth defect density [1–3,7,8,22–24,30,31]. Fig. 7 shows potentiodynamic polarisation curves for the CrN/NbN nano-scale multilayer coatings.

In general, all coated specimens (above E_{corr} value) exhibited an increase in corrosion currents with increasing anodic potentials. This can be attributed to the dissolution of Cr phase (from the coating and/or the substrate) as well as corrosion of the substrate [31], since Nb has been found to be passive at these conditions of pH and potentials.

In general all the coatings show increased fluctuation in corrosion currents in the anodic potential ranges of around 50 mV and 400 mV. This fluctuation was observed to be severe for the thinnest coating (0.281 µm). Considering the thin and uneven nature of this coating (Fig 2a-b) it can be speculated that with increasing anodic potential and hence time, there was an increase in the number of sites where coating dissolution took place leading to the exposure of the substrate. In optical microscopic images of the CrN/NbN, coating surfaces were found to be severely damaged, with large pits visually evident. Thus the corrosion current fluctuation was a result of active dissolution, passivation, trans-passivation and re-passivation events happening on the newly exposed substrate surfaces through pits as well as the coating. With the increase of coating thickness the rapid occurrence of these events is reduced, for e.g., as observed for 0.56 µm thick coating only to be compensated, to some extent, by defects in the coatings which were preferentially removed by the galvanic effects [22,30,31]. The corrosion response observed in 2.15 µm thick coating was purely due to the events of the corrosion/passivation of the coating. As evident, though the number of defects increased with coating thickness, the corrosion tests suggested that these defects were not extended throughout the thickness hence originated during the intermediate stage of coating deposition. Any defect initiated at the substrate level, could act as a direct pathway for corrosive media to reach the substrate and increase the corrosion rate significantly.

Fig. 8 shows the potentiodynamic polarisation curve for the UBM coating as well as the HIPIMS/UBM coating of similar thickness. It is clearly visible that in the electrochemical potential range of -400 mV to +400 mV the corrosion current density significantly is higher compared to that of HIPIMS/UBM coatings. So these studies indicated that the coating

removal rate i.e, the corrosion rate of the HIPIMS/UBM coating was lower than the UBM coating. This result shows the similar trend with the previous study [22]. Interestingly, the defect density of the UBM coatings was much lower than the HIPIMS/UBM coatings. However, the superior microstructure (inter columnar void free) of HIPIMS/UBM coatings makes the coating protective despite of having growth defects.

Conclusions

CrN/NbN multilayer coatings were deposited in an industrial sized PVD machine with the help of HIPIMS/UBM technique to study their morphology and growth defects. It was achieved by the selection of suitable HIPIMS power supply parameters as well as effective use of arc suppression units on cathode and bias power supplies. No evidence of droplet formation and its deposition at any stage of coating process was observed, i.e. during etching of the substrate or deposition of multilayers. Comprehensive study of the coating surfaces and cross-sections suggests that some type of defects were generated due to the interruption of the systematic coating growth by external factors such as chamber dust or substrate surface imperfections such as pits or protrusions. These defects are common in PVD techniques and that use of HIPIMS did not lead to generation of a new category of defect. The density of these defects increased with thickness of the coating. However, irrespective of the thickness, the coating was very dense and free from inter-columnar voids, usually associated with low energy deposition conditions such as low bias and deposition temperatures. Results from corrosion experiments revealed that though visible on the surface, these defects may not extend all the way to the substrate thereby providing effective barrier against a corrosive medium.

Acknowledgement

This study was carried out within a PhD research programme. The financial support by Zimmer-Biomet is gratefully acknowledged.

Reference

[1] D.B. Lewis, S.J. Creasey, C. Wustefeld, A.P. Ehiasarian, P.E. Hovsepian, The role of the growth defects on the corrosion resistance of CrN/NbN superlattice coatings deposited at low temperatures, Thin Solid Films 503 (2006) 143–148.

[2] P. Panjan, M. Čekada, M. Panjan, D. Kek-Merl, Growth defects in PVD hard coatings, Vacuum 84 (2009) 209–214.

[3] P. Panjan, M. Čekada, M. Panjan, D. Kek-Merl, F. Zupanič, L. Čurković, S. Paskvale, Surface density of growth defects in different PVD hard coatings prepared by sputtering, Vacuum 86 (2012) 794–798.

[4] A. Drnovšek, P. Panjan, M. Panjan, M. Čekada, The influence of growth defects in sputter-deposited TiAlN hard coatings on their tribological behavior, Surf. Coatings Technol. 288 (2016) 171–178.

[5] W.-D. Münz, I.J. Smith, D.B. Lewis, S. Creasey, Droplet formation on steel substrates during cathodic steered arc metal ion etching, Vacuum 48 (1997) 473–481.

[6] W.-D. Münz, Comparison of TiAlN coatings grown by unbalanced magnetron and arc bond sputtering techniques, J. Vac. Sci. Technol. A 11 (1993) 2583-2589.

[7] H.W. Wang, M.M. Stack, S.B. Lyon, P. Hovsepian, W.D. Münz, The corrosion behaviour of macroparticle defects in arc bond-sputtered CrN/NbN superlattice coatings, Surf. Coat. Technol. 126 (2000) 279–287.

[8] J.G.Han, S.H. Ahn, J.H. Lee, J.G. Kim, Localized corrosion mechanisms of the multilayered coatings related to growth defects, Surf. Coat. Technol. 177–178 (2004) 638–644.

[9] M. Čekada, P. Panjan, D. Kek-Merl, M. Panjan, G. Kapun, SEM study of defects in PVD hard coatings, Vacuum 82 (2007) 252–256.

[10] P. Panjan, P. Gselman, D. Kek-Merl, M. Čekada, M. Panjan, G. Dražić, T. Bončina, F. Zupanič, Growth defect density in PVD hard coatings prepared by different deposition techniques, Surf. Coat. Technol. 237 (2013) 349–356.

[11] D.D. La Grange, N. Goebbels, A. Santana, R. Heuberger, T. Imwinkelried, L. Eschbach, A. Karimi, Effect of niobium onto the tribological behavior of cathodic arc deposited Nb–Ti–N coatings, Wear 368–369 (2016) 60–69.

[12] I. Zhirkov, A. Petruhins, J. Rosen, Effect of cathode composition and nitrogen pressure on macroparticle generation and type of arc discharge in a DC arc source with Ti-Al compound cathodes, Surf. Coat. Technol. 281 (2015) 20–26.

[13] A. Anders, Physics of arcing, and implications to sputter deposition, Thin Solid Films 502 (2006) 22–28.

[14] A.P. Ehiasarian, J.G. Wen, I. Petrov, Interface microstructure engineering by high power impulse magnetron sputtering for the enhancement of adhesion, J. Appl. Phys. 101 (2007) 054301.

[15] A.P. Ehiasarian, W.D. Münz, High power pulsed magnetron sputtered CrN x films, Surf. Coat. Technol. 163–164 (2003) 267–272.

[16] P.E. Hovsepian, A.A. Sugumaran, Y. Purandare, D. A.L. Loch, A.P. Ehiasarian, Effect of the degree of high power impulse magnetron sputtering utilisation on the structure and properties of TiN films, Thin Solid Films 562 (2014) 132–139.

[17] T. Hurkmans, D.B. Lewis, J.S. Brooks, W.D. Münz, Chromium nitride coatings grown by unbalanced magnetron (UBM) and combined arc/unbalanced magnetron (ABS^{TM}) deposition techniques, Surf. Coat. Technol. 86–87 (1996) 192–199.

[18] A.P. Ehiasarian, Y.A. Gonzalvo, T.D. Whitmore, Time-resolved ionisation studies of the high power impulse magnetron discharge in mixed argon and nitrogen atmosphere, Plasma Process. Polym. 4 (2007) 309–313.

[19] A.P. Ehiasarian, Fundamentals and applications of HIPIMS, in: R. Wei (Ed.), Plasma Surface Engineering Research and its Practical Applications, Research Signpost, Trivandrum, India, 2008: pp. 35–86.

[20] F. Magnus, O.B. Sveinsson, S. Olafsson, J.T. Gudmundsson, Current-voltage-time characteristics of the reactive Ar/N2 high power impulse magnetron sputtering discharge, J. Appl. Phys. 110 (2011) 083306.

[21] P.E. Hovsepian, D.B. Lewis, W.D. Münz, Recent progress in large scale manufacturing of multilayer/superlattice hard coatings, Surf. Coat. Technol. 133–134 (2000) 166–175.

[22] Y.P. Purandare, A.P. Ehiasarian, M.M. Stack, P.E. Hovsepian, CrN/NbN coatings deposited by HIPIMS: A preliminary study of erosion-corrosion performance, Surf. Coat. Technol. 204 (2010) 1158–1162.

[23] P.E. Hovsepian, D.B. Lewis, W.D. Münz, S.B. Lyon, M. Tomlinson, Combined cathodic arc/unbalanced magnetron grown CrN/NbN superlattice coatings for corrosion resistant applications, Surf. Coat. Technol. 120–121 (1999) 535–541.

[24] M. Tomlinson, S.B. Lyon, P. Hovsepian, W.D. Munz, Corrosion performance of CrN/NbN superlattice coatings deposited by the combined cathodic arc/unbalanced magnetron technique, Vacuum 53 (1999) 117–121.

[25] A.P. Ehiasarian, P.Eh.Hovsepian, W-D. Munz, Combined coating process comprising magnetic field-assisted, high-power, pulsed cathode sputtering and an unbalanced magnetron, Patent US7081186 B2 (25 Jul 2006), EP1260603 A2 (27 Nov 2002), DE10124749 A1 (28 Nov 2002).

[26] P.E. Hovsepian, A.P. Ehiasarian, Y.P. Purandare, B. Biswas, F.J. Pérez, M.I. Lasanta, M.T. De Miguel, A. Illana, M. Juez-Lorenzo, R. Muelas, A. Agüero, Performance of HIPIMS deposited CrN/NbN nanostructured coatings exposed to

650°C in pure steam environment, Mater. Chem. Phys. 179 (2016) 110–119.

[27] Y.P. Purandare, A.P. Ehiasarian, P.E. Hovsepian, Deposition of nanoscale multilayer CrN/NbN physical vapor deposition coatings by high power impulse magnetron sputtering, J. Vac. Sci. Technol. A 26 (2008) 288-296.

[28] A.P. Ehiasarian, A. Vetushka, Y.A. Gonzalvo, G. Sáfrán, L. Székely, P.B. Barna, Influence of high power impulse magnetron sputtering plasma ionization on the microstructure of TiN thin films, J. Appl. Phys. 109 (2011) 104314.

[29] J.A. Thornton, High Rate Thick Film Growth, Annu. Rev. Mater. Sci. 7 (1977) 239–260.

[30] P.E. Hovsepian, D.B. Lewis, Q. Luo, A. Farinotti, Corrosion resistance of CrN/NbN superlattice coatings grown by various physical vapour deposition techniques, Thin Solid Films. 488 (2005) 1–8.

[31] M. Pourbaix, Atlas of electrochemical equilibria in aqueous solutions, National Association of Corrosion Engineers, Houston, Tex., 1974.

Figure caption

Fig. 1. (a) AFM image, (b) Low magnification and (c) High magnification SEM image of ion etched sample.

Fig. 2. (a) AFM image and (b) SEM image of 15 minutes deposited coating; (c) AFM image and (d) SEM image of 30 minutes deposited coating; (e) AFM image and (f) SEM image of 60 minutes deposited coating; (g) AFM image and (h) SEM image of 120 minutes deposited coating produced using HIPIMS/UBM.

Fig. 3. (a) Cross section of nodular defect, (b) open void defect, (c) pinhole defects, (d) cone-like defect, (e) pinhole defect in UBM coating deposited for 100 min, (f) top view of a HIPIMS/UBM coating deposited for 120 minutes, (g) top view of a commercially available CrN/NbN coating deposited by arc-PVD technique, (h) droplet defect on an arc-PVD coating.

Fig. 4. (a) Plan view of the nodular defect, (b) Cross sectional view after ion beam milling, (c) Magnified image of defect cross section.

Fig. 5. (a). Thickness variation of the HIPIMS/UBM coatings with the deposition time and the related cross-section SEM images. (b) Cross-section SEM image of the UBM coating.

Fig. 6. Coating thickness vs. Percentage of surface area covered by imperfections (A_d).

Fig. 7. Potentiodynamic polarisation curves for the HIPIMS/UBM CrN/NbN nano-scale multilayer coatings.

Fig. 8. Potentiodynamic polarisation curves for the CrN/NbN nano-scale multilayer coatings of similar thicknesseses deposited by HIPIMS/UBM and pure UBM.

Table Caption

Table 1. Roughness measurements of the polished, etched and coated samples.

Samples	**Roughness Ra (µm)**
Polished SS substrate	0.012
Etched Substrate	0.023
HIPIMS/UBM Coating (deposition time = 15 minutes)	0.021
HIPIMS/UBM Coating (deposition time = 30 minutes)	0.018
HIPIMS/UBM Coating (deposition time = 60 minutes)	0.038
HIPIMS/UBM Coating (deposition time = 120 minutes)	0.039
HIPIMS/UBM Coating (deposition time = 120 minutes) After cleaning the chamber	0.031
UBM Coating (deposition time = 100 minutes) After cleaning the chamber	0.022

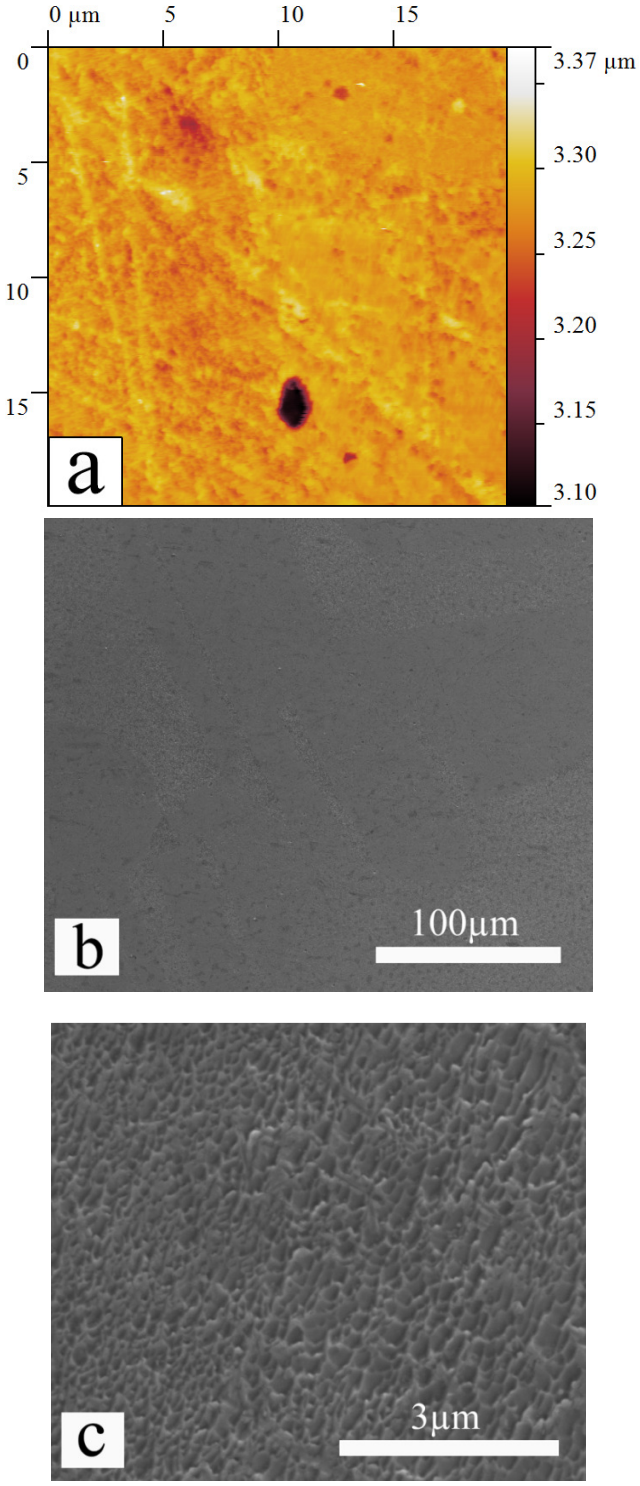

Fig. 1. (a) AFM image, (b) Low magnification and (c) High magnification SEM image of ion etched sample.

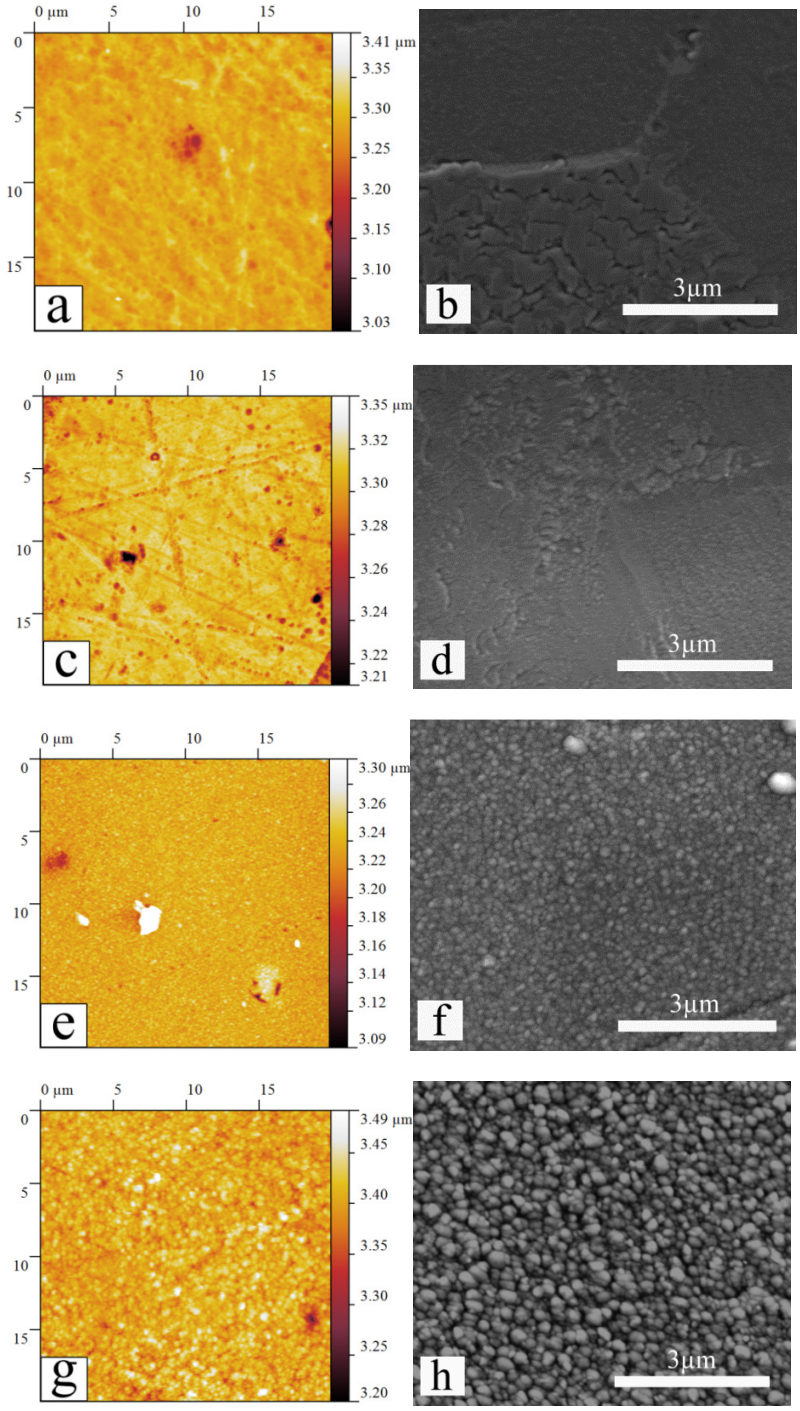

Fig. 2. (a) AFM image and (b) SEM image of 15 minutes deposited coating; (c) AFM image and (d) SEM image of 30 minutes deposited coating; (e) AFM image and (f) SEM image of 60 minutes deposited coating; (g) AFM image and (h) SEM image of 120 minutes deposited coating produced using HIPIMS/UBM.

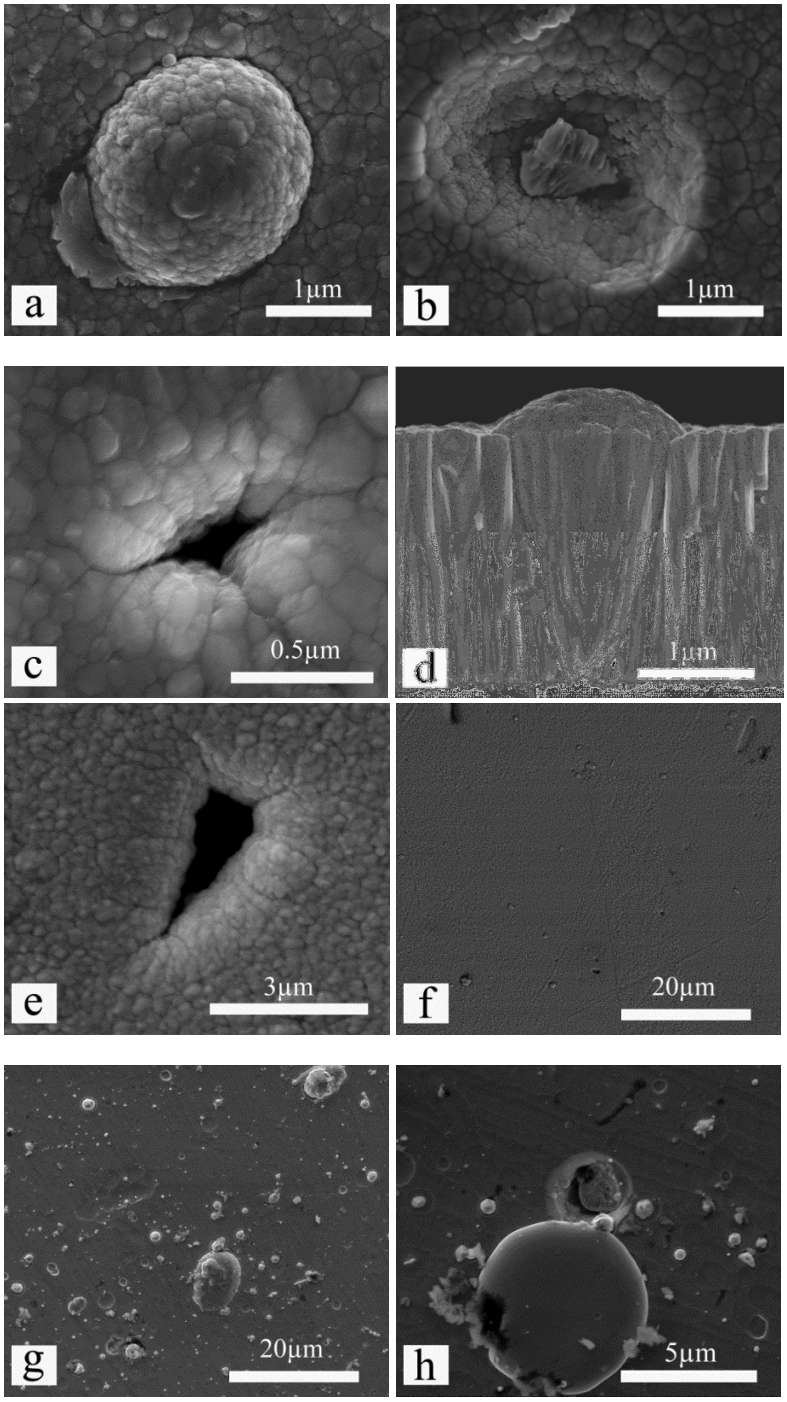

Fig. 3. (a) Cross section of nodular defect, (b) open void defect, (c) pinhole defects, (d) cone-like defect, (e) pinhole defect in UBM coating deposited for 100 min, (f) top view of a HIPIMS/UBM coating deposited for 120 minutes, (g) top view of a commercially available CrN/NbN coating deposited by arc-PVD technique, (h) droplet defect on an arc-PVD coating.

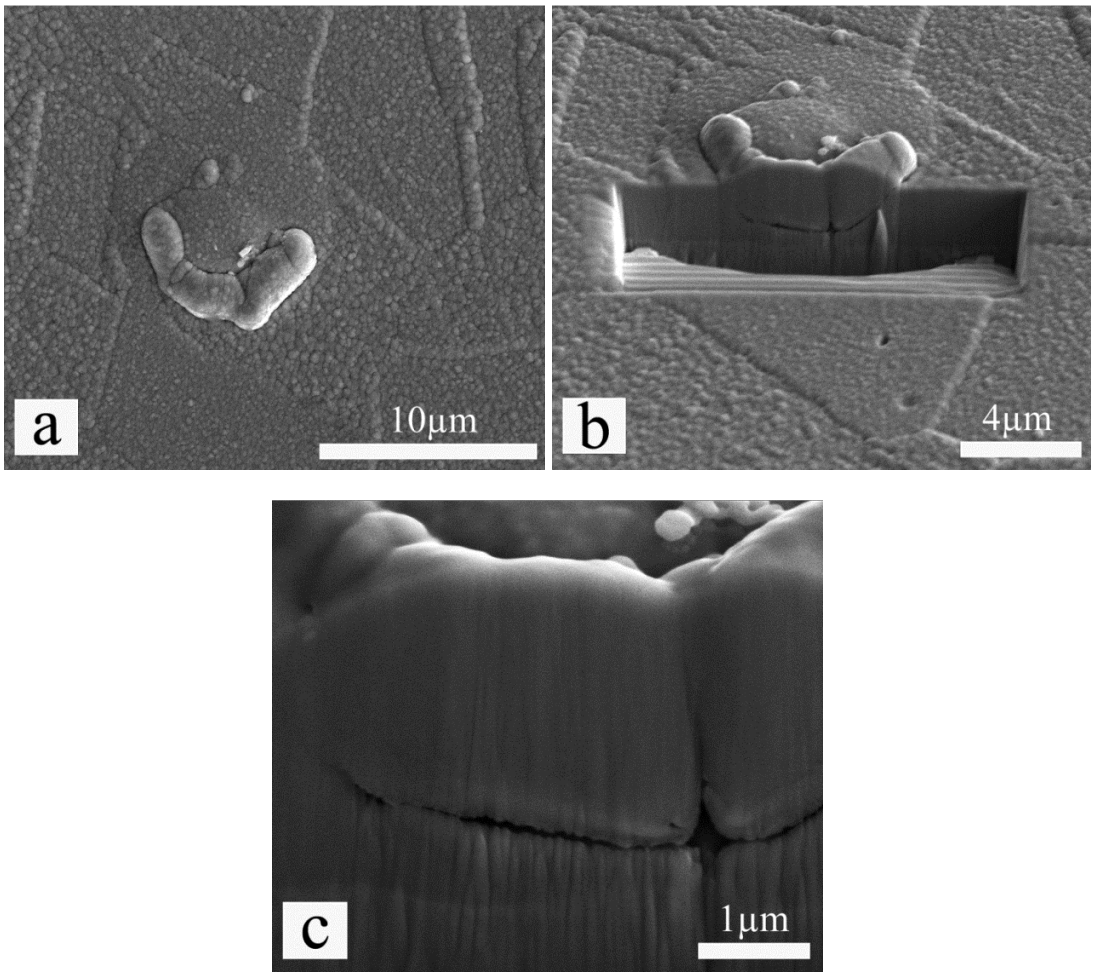

Fig. 4. (a) Plan view of the nodular defect, (b) Cross sectional view after ion beam milling, (c) Magnified image of defect cross section.

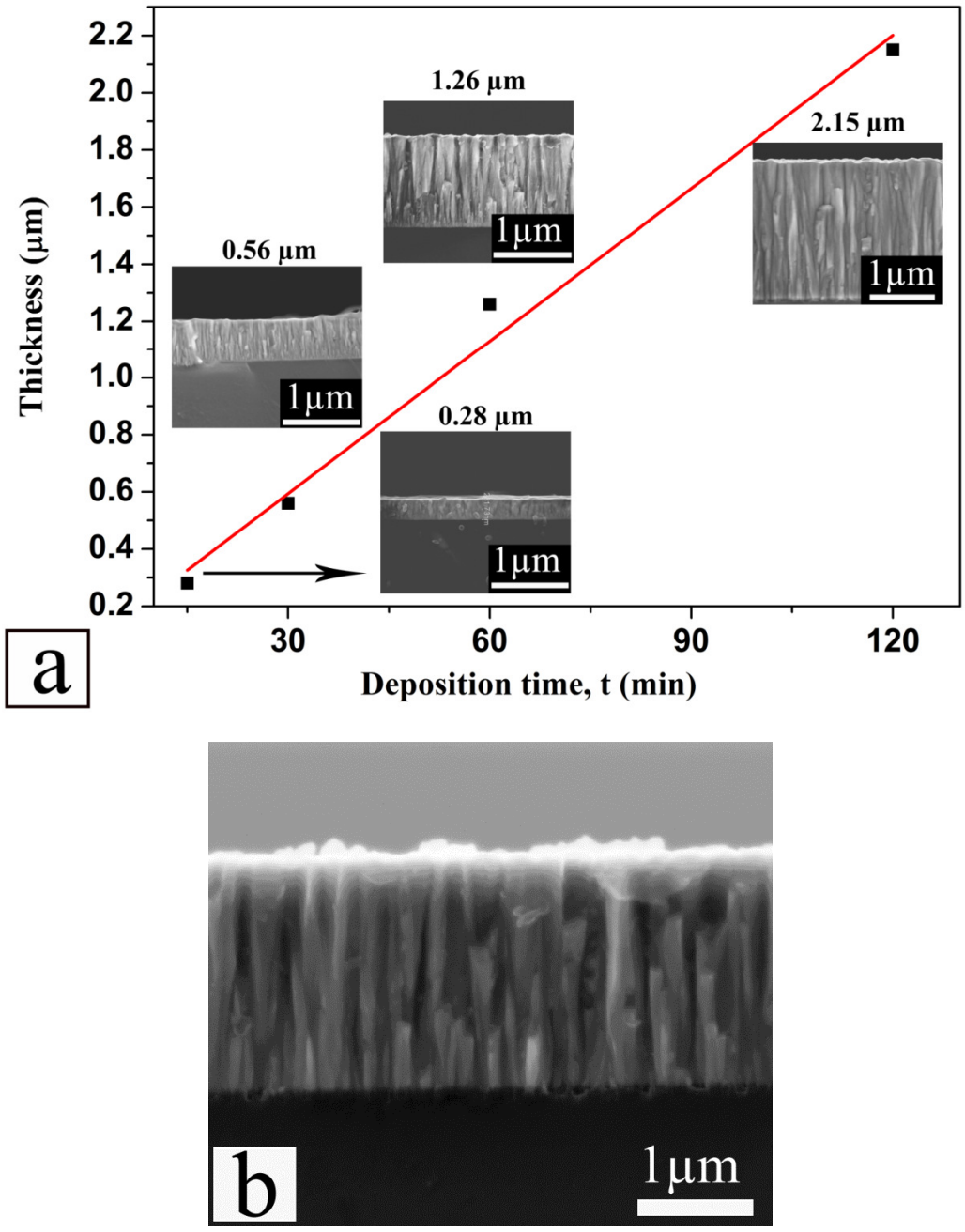

Fig. 5. (a). Thickness variation of the HIPIMS/UBM coatings with the deposition time and the related cross-section SEM images. (b) Cross-section SEM image of the UBM coating.

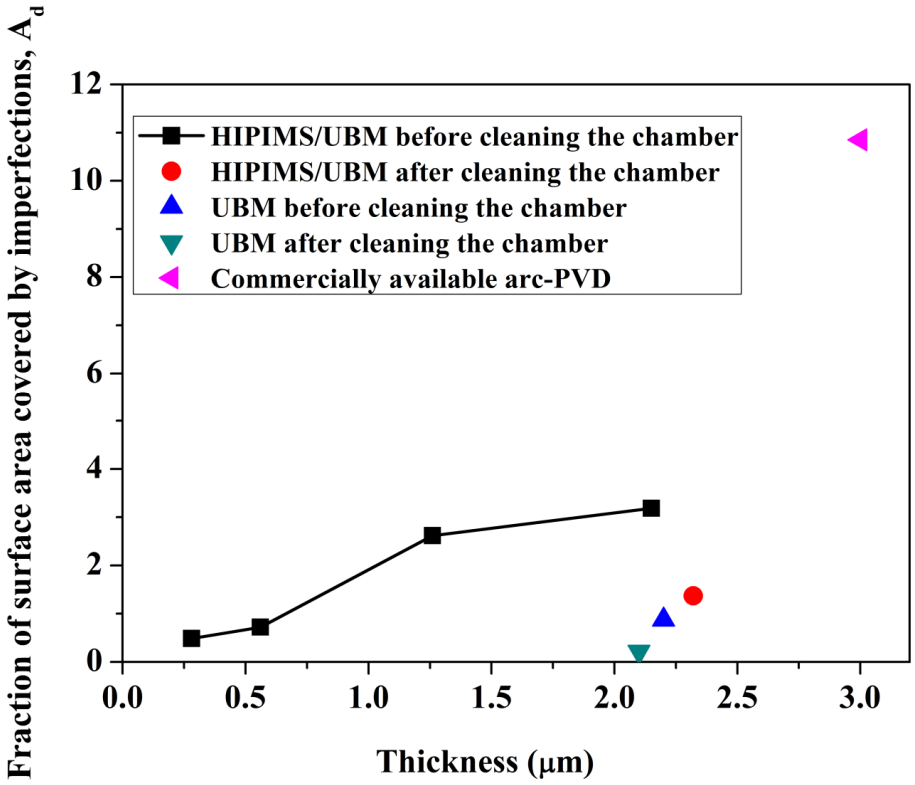

Fig. 6. Coating thickness vs. Percentage of surface area covered by imperfections (A_d).

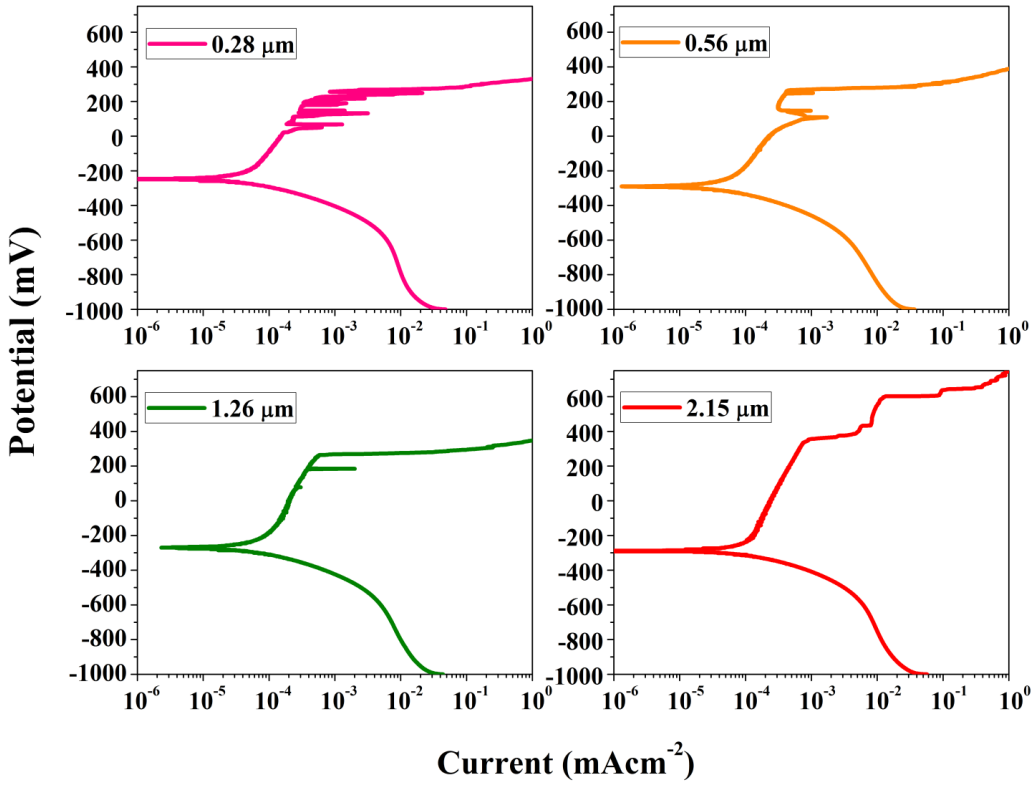

Fig. 7. Potentiodynamic polarisation curves for the HIPIMS/UBM CrN/NbN nano-scale multilayer coatings.

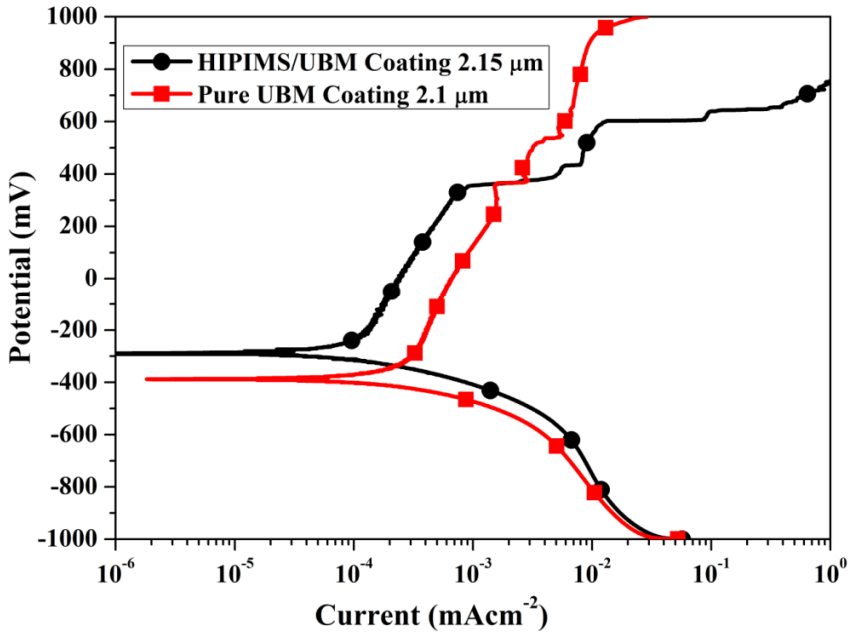

Fig. 8. Potentiodynamic polarisation curves for the CrN/NbN nano-scale multilayer coatings of similar thicknesseses deposited by HIPIMS/UBM and pure UBM.